Journal of Solid State Chemistry **158**, 307–314 (2001)
doi:10.1006/jssc.2001.9111, available online at http://www.idealibrary.com on IDEAL®

Synthesis, Crystal Chemistry, and Electrical and Magnetic Properties of $Sr_3Fe_{2-x}Co_xO_{7-\delta}$ ($0 \leq x \leq 0.8$)

F. Prado and A. Manthiram[1]

Texas Materials Institute, ETC 9.104, The University of Texas at Austin, Austin, Texas 78712

Received October 24, 2000; in revised form January 2, 2001; accepted January 19, 2001; published online April 5, 2001

$Sr_3Fe_{2-x}Co_xO_{7-\delta}$ oxides crystallizing in a tetragonal perovskite-related intergrowth structure have been synthesized for $0 \leq x \leq 0.8$ and characterized by X-ray powder diffraction, wet-chemical analysis, and electrical and magnetic measurements. The lattice parameters, oxygen content, and average oxidation state of iron and cobalt decrease with increasing Co content x. However, the samples show instability on exposure to ambient air for prolonged periods of time due to a possible reaction with H_2O and CO_2. Resistivity measurements indicate that the samples exhibit a semiconducting behavior at low temperatures ($80 \leq T \leq 680$ K) and the resistivity value decreases with increasing Co content. For $T > 680$ K, the resistivity versus temperature plots exhibit a change in the sign of the slope from negative to positive due to oxygen loss at higher temperatures. Low-temperature resistivity data show an exponential temperature dependence of $\rho \propto \exp(T_0/T)^{\nu}$ with $\nu = \frac{1}{2}$ for samples with $0 \leq x \leq 0.25$ and $\nu = \frac{1}{4}$ for samples with $0.6 \leq x \leq 0.8$ suggesting a transition from activated carriers involving a coulomb gap to thermally activated hopping as the Co content increases. SQUID magnetometer measurements indicate a transition from antiferromagnetic behavior to weak ferromagnetic behavior as the Co content increases. © 2001 Academic Press

1. INTRODUCTION

The discovery of high-T_c superconductivity in layered copper oxides having perovskite-related intergrowth structures (1) has intensified during the past decade the investigation of the structure–property relationships of 3d transition metal oxides. Some of the perovskite-related 3d transition metal oxides exhibit interesting electrical and magnetic properties due to the existence of small energy gaps either between the O:2p and metal:3d levels (charge transfer insulator) or between the lower and upper Hubbard bands (Mott–Hubbard insulator). The perovskite oxides have also drawn much attention recently due to the discovery of colossal magnetoresistance in the $La_{1-x}A_xMnO_3$ (A = Sr, Ca, Ba) system (2), and high oxygen permeation rates in the family of mixed electronic–ionic conductors $La_{1-x}Sr_xFe_{1-y}Co_yO_3$ (3).

Strontium iron oxides with iron in the 3+/4+ oxidation state form a Ruddlesden–Popper series of intergrowth oxides having the general formula $Sr_{n+1}Fe_nO_{3n+1}$. Among them, the crystal structure of the $n = 2$ member $Sr_3Fe_2O_7$ can be described as having layers stacked along the c-axis with two $SrFeO_3$ perovskite layers alternating with a SrO rock-salt layer (Fig. 1). The $Sr_3Fe_2O_{7-\delta}$ phase exhibits a wide range of oxygen nonstoichiometry $0 \leq \delta \leq 1$ without undergoing any change in the symmetry of the crystal structure (4). Electrical transport (5) and magnetic measurements (5–8) have shown that $Sr_3Fe_2O_{7-\delta}$ is a semiconductor and it orders antiferromagnetically at low temperatures for the whole range of oxygen nonstoichiometry ($0 \leq \delta \leq 1$). Additionally, Mossbauer spectroscopy of $Sr_3Fe_2O_7$ has indicated a charge density wave corresponding to the disproportionation of Fe^{4+} into Fe^{5+} and Fe^{3+} (5–7). More recently, Adler *et al.* (6) have reported a pressure-driven insulator to metal transition in $Sr_3Fe_2O_7$ at $P \approx 20$ GPa. Adler *et al.* (6) have suggested that the application of high pressure strengthens the Fe(3d)–O(2p)–Fe(3d) covalent interaction and thereby leads to a closing of the charge density wave gap in the σ^* conduction band.

Structural and magnetic properties have also been reported for $ALn_2Fe_2O_7$ (A = Sr or Ba and Ln = lanthanide) (9, 10), $Sr_{2.6}Ba_{0.4}Fe_2O_{7-\delta}$ (5) and $Sr_{2.7}La_{0.3}Fe_2O_{7-\delta}$ (5) in which the A-site has been partially substituted by lanthanides. Additionally, substitution of Ru for Fe in the B site has also been studied by Battle *et al.* (11). Sr_3FeRuO_7 has been found to exhibit a spin glass behavior. However, little or no attempts have been made to study the effect of substitution of Co for Fe on the properties of $Sr_3Fe_2O_{7-\delta}$. Recently, we investigated the effect of Co substitution on the oxygen permeation properties of $Sr_{3-x}La_xFe_{2-y}Co_yO_{7-\delta}$ (12, 13) and $LaSr_3Fe_{3-x}Co_xO_{10-\delta}$ (14). The Co substitution was found to improve both the electronic and oxide-ion conductivity at high temperatures resulting in higher oxygen permeation flux values. The increase in electronic conductivity and oxygen permeation flux was attributed to

[1] To whom correspondence should be addressed.

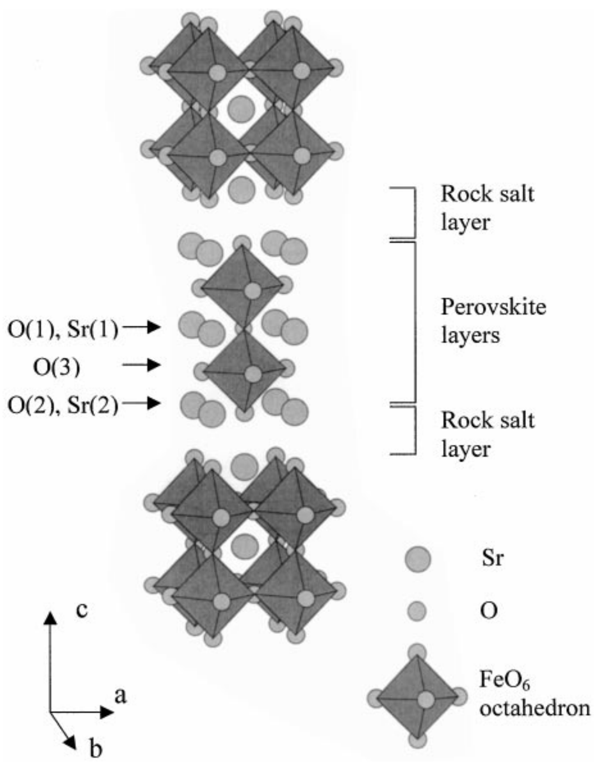

FIG. 1. Crystal structure of $Sr_3Fe_2O_7$.

the increase in the covalency of the $B(3d)$–$O(2p)$ bond. We present in this paper the effect of Co substitution on the crystal chemistry, electrical conductivity, and magnetic properties of the $Sr_3Fe_{2-x}Co_xO_{7-\delta}$ system. During the review process of this manuscript, we also came across another study by Ghosh and Adler (15) reporting the substitution of 10% Co for Fe to obtain $Sr_3Fe_{1.8}Co_{0.2}O_{\sim 7}$. They have reported a large negative magnetoresistance effect at low temperatures (45% at 5 K and 9 T) for this composition and suggested the existence of strong ferromagnetic and competing antiferrromagnetic interactions leading to a cluster-glass-like magnetic behavior.

2. EXPERIMENTAL

The $Sr_3Fe_{2-x}Co_xO_{7-\delta}$ samples with $0 \leq x \leq 1.0$ were prepared by a solid-state reaction of $SrCO_3$, Fe_2O_3, and Co_3O_4. Required quantities of the raw materials were ground and calcined first at 900°C for 12 h in air. The mixture was then reground, pressed into pellets, and fired at 1300°C for 24 h in air. The samples were then divided into two sets and subjected to a post-heat treatment. The first set of samples were heated at 900°C for 1 h in air, cooled at a rate of 1°C/min to 500°C, maintained at 500°C for 6 h and then cooled to room temperature at a rate of 1°C/min. This set of samples is designated as "air-annealed samples." The second set of samples were also subjected to a similar heat treatment procedure, but in oxygen atmosphere instead of air. This set of samples is designated as "oxygen-annealed samples."

The samples were characterized by X-ray powder diffraction recorded with a Phillips APD 3520 diffractometer using Cu$K\alpha$ radiation and a graphite monochromator. The X-ray data were collected with a counting time of 10 s per 0.02° and refined by the Rietveld method with the DBWS-9411 program (16). The oxidation state of (Fe, Co) and the oxygen content were determined by iodometric titration (17). Thermogravimetric analysis (TGA) plots were recorded with a Perkin-Elmer Series 7 thermal analyzer with a heating rate of 1°C/min in a flowing mixture of 80% N_2 and 20% O_2. High-temperature ($450 \leq T \leq 1213$ K) conductivity measurements were carried out in air with disc samples using a four-probe dc technique with the Van der Pauw configuration. Low-temperature ($80 \leq T \leq 300$ K) conductivity measurements were carried out with bar-shaped samples with a four-probe technique. Magnetic measurements were carried out with a Quantum design SQUID magnetometer in the temperature range $5 \leq T \leq 320$ K.

3. RESULTS AND DISCUSSION

Figure 2 shows the X-ray powder diffraction patterns of the oxygen-annealed $Sr_3Fe_{2-x}Co_xO_{7-\delta}$ samples for

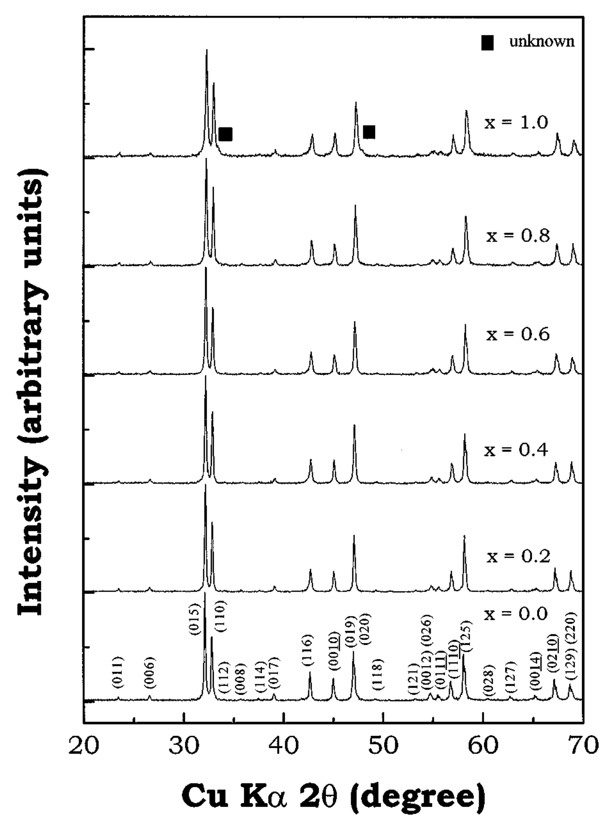

FIG. 2. X-ray powder diffraction patterns of the oxygen-annealed $Sr_3Fe_{2-x}Co_xO_{7-\delta}$ samples.

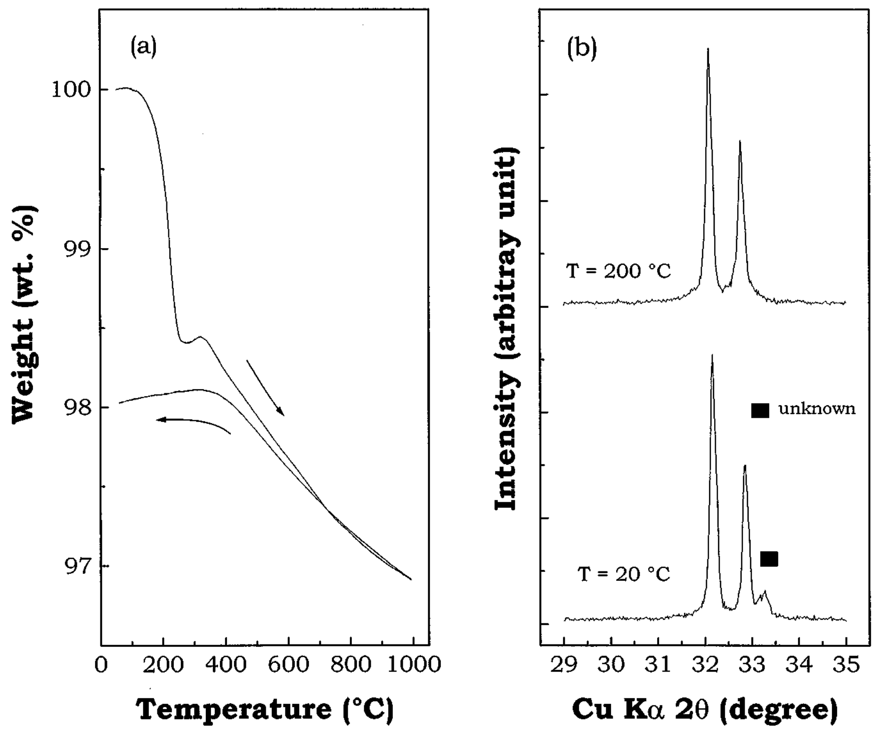

FIG. 3. (a) TGA plot of the $Sr_3Fe_2O_{7-\delta}$ sample. The plot was recorded in a gas mixture of 20% O_2 and 80% N_2 with heating and cooling rates of 1°C/min. (b) X-ray diffraction pattern of the $Sr_3Fe_2O_{7-\delta}$ sample at room temperature and $T = 200$°C. Prior to the TGA and X-ray experiments, the sample had been exposed to the ambient atmosphere for several days.

$0 \leq x \leq 1.0$. The data indicate that single phase samples are formed for $0 \leq x \leq 0.8$. For the $x = 1$ sample, the presence of a small peak at $2\theta = 33.7°$ suggests the formation of an unknown secondary phase. However, all the samples were found to experience instability in ambient air at room temperature. Figure 3a shows the TGA plot of the $x = 0$ sample that has been previously exposed to ambient air at room temperature for several days. The TGA data show that the sample loses weight in two steps during heating. The first step is between room temperature and 250°C, and the second step is between 300 and 900°C. While the weight loss corresponding to the second step is nearly reversible, that corresponding to the first step is irreversible. Figure 3b shows the X-ray diffraction patterns of this sample recorded at room temperature and at 200°C. While the pattern recorded at room temperature shows an extra reflection around $2\theta = 33.5°$ corresponding to a secondary phase, the pattern recorded at 200°C shows a single phase $Sr_3Fe_2O_{7-\delta}$ without the secondary phase. From this observation, we conclude that the secondary phase formed is due to the reaction of $Sr_3Fe_2O_{7-\delta}$ at room temperature with CO_2 or moisture present in ambient air. The reaction of the samples with ambient air and the formation of the secondary phase were found to become more pronounced with increasing Co content in $Sr_3Fe_{2-x}Co_xO_{7-\delta}$.

The lattice parameters of the $Sr_3Fe_{2-x}Co_xO_{7-\delta}$ phases were refined by the Rietveld method on the basis of the tetragonal space group *I*4/*mmm*. The variations of lattice parameters with Co content are shown in Fig. 4 for both the air-annealed and oxygen-annealed samples. The a and c parameters and the unit cell volume V decrease with increasing Co content due to a substitution of a smaller $Co^{3+/4+}$ for $Fe^{3+/4+}$. For a given Co content, the oxygen-annealed samples have smaller a and c parameters and cell volume compared to the air-annealed samples due to a higher oxygen content and oxidation state for (Fe, Co) (see below).

Figure 5 shows the variations of the oxygen content and the average oxidation state of (Fe, Co) with the Co content in $Sr_3Fe_{2-x}Co_xO_{7-\delta}$. All the samples show oxygen contents of less than 7.00, but the oxygen-annealed samples have higher oxygen contents than the air-annealed samples. The oxygen content values of the $x = 0$ samples are in close agreement with that reported previously for samples annealed in air and oxygen (4, 18). The oxygen content and the average oxidation state of (Fe, Co) decrease slightly as the Co content increases. This is due to the difficulty of stabilizing Co^{4+} compared to Fe^{4+}.

Figures 6a and 6b show the temperature variations of the electrical resistivity (ρ) in the low ($75 \leq T \leq 300$ K)- and high ($450 \leq T \leq 1200$ K)-temperature regions, respectively,

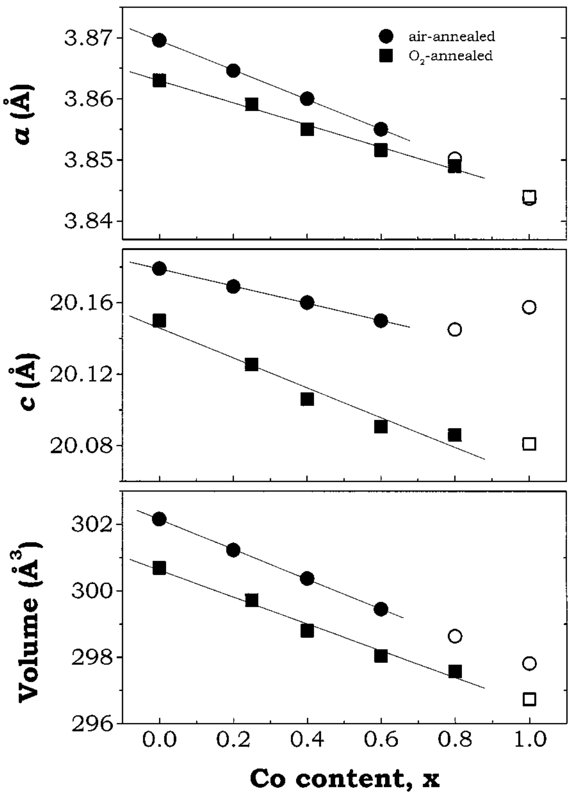

FIG. 4. Variations of lattice parameters and cell volume of air-annealed and oxygen-annealed $Sr_3Fe_{2-x}Co_xO_{7-\delta}$ samples with Co content x. Open symbols refer to samples showing an unknown secondary phase.

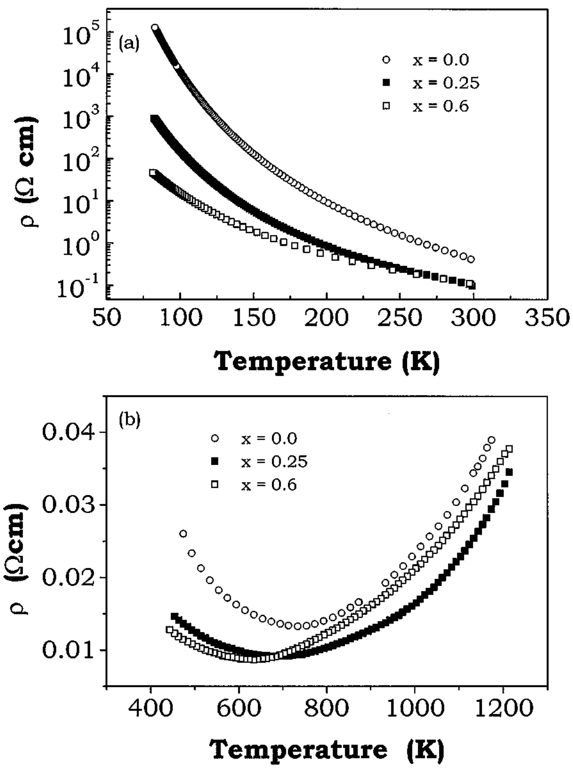

FIG. 6. Temperature dependence of the resistivity of air-annealed $Sr_3Fe_{2-x}Co_xO_{7-\delta}$ samples in air: (a) low temperature region ($80 \le T \le 300$ K and (b) high-temperature region ($450 \le T \le 1250$ K).

for $Sr_3Fe_{2-x}Co_xO_{7-\delta}$ with $0 \le x \le 0.6$. The resistivity measurements (Fig. 6a) were carried out with the air-annealed samples. In the low-temperature region, ρ decreases as T increases, indicating a semiconducting behavior for all the samples. In the higher temperature region, the ρ versus

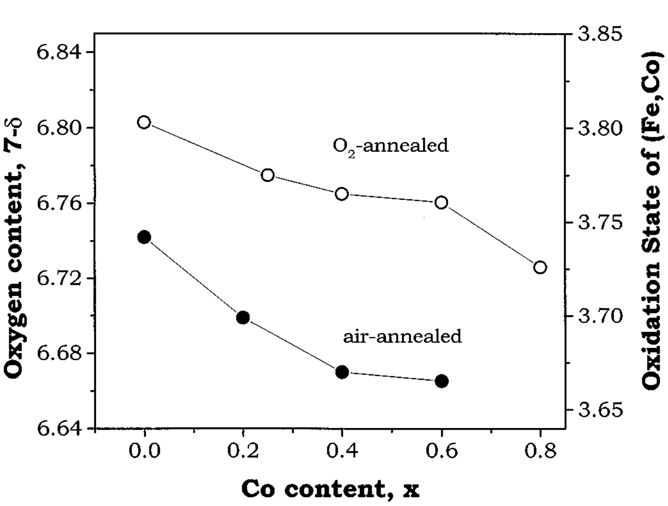

FIG. 5. Variation of oxygen content and average oxidation state of Fe and Co with Co content in $Sr_3Fe_{2-x}Co_xO_{7-\delta}$.

T curves exhibit a change in the sign of the slope with a resistivity minimum at a temperature $630 \le T_t \le 730$ K. The value of T_t decreases with increasing Co content x in $Sr_3Fe_{2-x}Co_xO_{7-\delta}$.

In order to understand the origin of the change in slope in the ρ versus T curves, we carried out TGA measurements in air for air-annealed $Sr_3Fe_{2-x}Co_xO_{7-\delta}$ with $0 \le x \le 0.6$. Before the TGA experiments, the samples were dried in air at 200°C to remove any impurity phase formed by exposure to ambient air (see Fig. 3). The variations of oxygen content with temperature (obtained from TGA data) are shown in Fig. 7. The initial oxygen contents in Fig. 7 before the TGA experiments were obtained from iodometric titration (Fig. 5). The samples begin to lose oxygen around $T = 300$–350°C and the temperature at which oxygen loss begins to occur decreases with increasing Co content x. For a given temperature, the oxygen vacancy concentration δ increases with increasing Co content. This is due to the difficulty of stabilizing Co^{4+} compared to Fe^{4+} as we pointed out earlier. Previous neutron diffraction experiments of $Sr_3Fe_2O_{7-\delta}$ at room temperature have located the oxygen vacancies in the O(1) sites (Fig. 1) between the two FeO_2 sheets (4). However, the oxygen vacancies may be located in the O(2) and O(3) sites as well at high

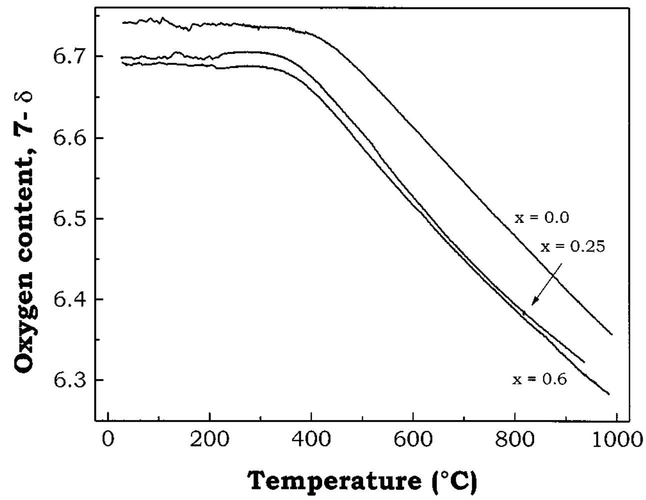

FIG. 7. TGA plots of the air-annealed $Sr_3Fe_{2-x}Co_xO_{7-\delta}$ samples recorded in a gas mixture of 20% O_2 and 80% N_2 with a heating rate of 1°C/min. The samples were predried in air at 200°C prior to the TGA experiments.

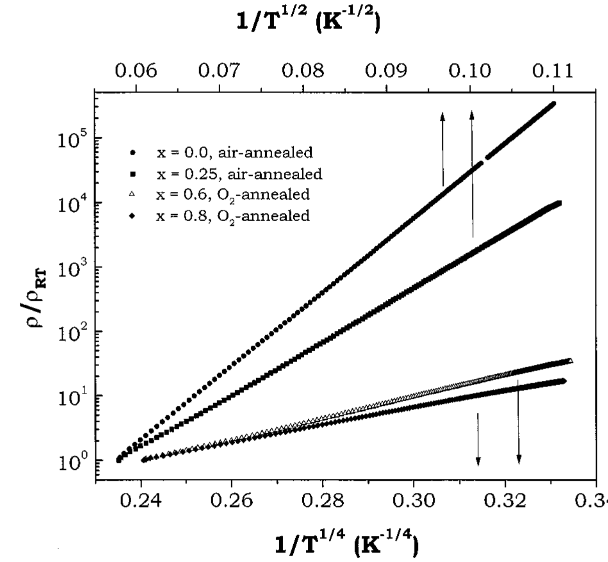

FIG. 9. $(1/T)^{1/n}$ dependence of the resistivity of air-annealed and oxygen-annealed $Sr_3Fe_{2-x}Co_xO_{7-\delta}$ samples.

temperatures. The TGA data in Fig. 7 suggest that the increase in resistivity with increasing temperature at $T > T_t$ in Fig. 6b is due to the loss of oxygen from the lattice. The increase in the concentration of oxygen vacancies results in an increase in the trapping of carriers and a lowering of carrier mobility which lead to an increase in resistivity, with temperature as found previously in the $La_{1-x}Sr_xFe_{1-y}Co_yO_{3-\delta}$ system (19).

Figure 8 displays the ρ/ρ_{RT} (RT refers to room temperature of 300 K) versus T curves in the low temperature $(75 \leq T \leq 300\ K)$ region for $Sr_3Fe_{2-x}Co_xO_{7-\delta}$ with $0 \leq x \leq 0.8$ and with different oxygen content values depending on whether the samples are air-annealed or oxygen-annealed. Although all the samples show a semiconducting behavior, the value of ρ/ρ_{RT} at $T \approx 80$ K decreases four orders of magnitude on going from the air-annealed $x = 0$ sample to the oxygen annealed $x = 0.8$ sample. Ghosh and Adler (15) have reported similar results for $Sr_3Fe_{1.8}Co_{0.2}O_{\sim 7}$. They found the low-temperature resistivity for this composition to be about 2 orders of magnitude lower than the $x = 0$ composition $Sr_3Fe_2O_{\sim 7}$. An analysis of the data in Fig. 8 using the relation,

$$\rho = \rho_0 e^{(T_0/T)^{1/n}}, \qquad [1]$$

indicates a change in the value of the parameter n from $n = 2$ to $n = 4$ on going from the air-annealed $x = 0.0$ to the oxygen-annealed $x = 0.8$ sample. This analysis is shown in Fig. 9. In Fig. 9, the ln (ρ/ρ_{RT}) versus $(1/T)^{1/2}$ $(n = 2)$ plots for the air-annealed $Sr_3Fe_{2-x}Co_xO_{7-\delta}$ samples with $x = 0$ and 0.25 exhibit a remarkable linearity in the whole temperature range. Similarly, the ln (ρ/ρ_{RT}) versus $(1/T)^{1/4}$ $(n = 4)$ plots for the oxygen-annealed $Sr_3Fe_{2-x}Co_xO_{7-\delta}$ samples with $x = 0.6$ and 0.8 exhibit a remarkable linearity in the whole temperature range in Fig. 9.

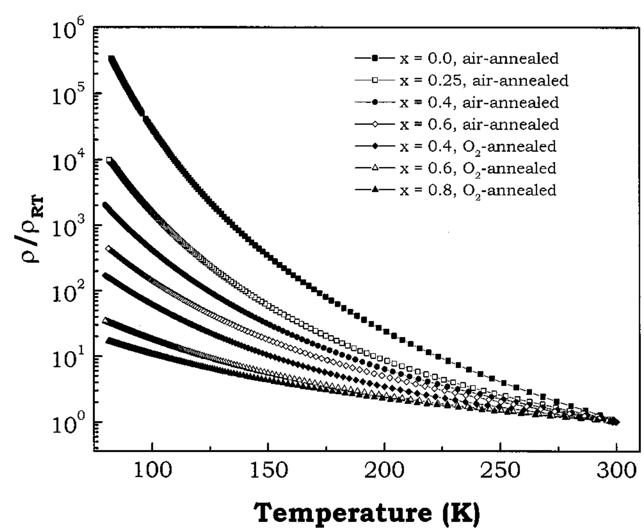

FIG. 8. Variations of ρ/ρ_{RT} with temperature for the air-annealed and oxygen-annealed $Sr_3Fe_{2-x}Co_xO_{7-\delta}$ samples.

Materials with semiconducting behavior exhibit a temperature dependence according to Eq. [1], in which the parameter n is related to the conduction process and it can have integer values between 1 and 4. A value of $n = 4$ is expected for a disordered system of electronic states localized close to the Fermi level (20). However, if the electron–electron interaction in these electronic states is significant, a coulomb gap may open at the Fermi level and a value of $n = 2$ is expected according to Efros and Shklovskii (21) for such a system. For example, a value of $n = 2$ has been reported previously for $Y_2SrCu_{0.6}Co_{1.4}O_{6.5}$ (22) at relatively higher temperatures $185 \le T \le 570$ K, and for $La_{1-x}Sr_xCoO_{3-\delta}$ with $0 \le x \le 0.2$ (23). The increase in the value of n from 2 to 4 with increasing Co content in the $Sr_3Fe_{2-x}Co_xO_{7-\delta}$ system suggests that the coulomb gap arising from correlation effects in the σ^* conduction band tends to close with increasing Co content. As we pointed out earlier, the substitution of Co for Fe increases the bandwidth w_σ of the σ^* conduction band due to a strengthening of the (Fe, Co)–O–(Fe, Co) covalent interaction and thereby decreases the coulomb gap. It is likely that the $Sr_3Fe_{2-x}Co_xO_{7-\delta}$ samples with higher Co content and with no oxygen vacancies may exhibit metallic behavior due to a closing of the coulomb gap.

Magnetic susceptibility measurements were carried out both with air-annealed and oxygen annealed $Sr_3Fe_{2-x}Co_xO_{7-\delta}$ ($0 \le x \le 0.8$) samples under zero-field-cooled (zfc) and field-cooled (fc) conditions. Figure 10 shows the variation of the molar magnetic susceptibility χ_m with temperature for the oxygen-annealed samples. As the Co content increases, the samples tend to exhibit spontaneous magnetization at lower temperatures, indicating a ferromagnetic behavior. The ferromagnetic ordering temperatures T_c computed from the data in Fig. 10 are given in Table 1. The T_c value and the spontaneous magnetization increase with increasing Co content until $x = 0.6$. For example, the field-cooled χ_m value at 5 K increases by two orders of magnitude on increasing the Co content x from 0 to 0.6. However, the sample with $x = 0.8$ exhibits lower spontaneous magnetization than the sample with $x = 0.6$. This could be due to a partial decomposition of the $x = 0.8$ sample originating from a chemical instability of these compounds as the Co content increases. The zero-field-cooled χ_m versus T curves show a maximum at a temperature $T_g < T_c$, suggesting a spin-glass or cluster-glass behavior due to competing ferromagnetic and antiferromagnetic interactions (15). The value of T_g increases slightly with increasing Co content (Table 1).

TABLE 1
Magnetic Data of $Sr_3Fe_{2-x}Co_xO_{7-\delta}$

Co content, x	Annealing atmosphere	Oxidation state of (Fe, Co)	μ_{eff} (μ_B)	θ (K)	T_c(K)[a]	Tg(K)[b]
0	Air	3.74	5.33	− 18	—	—
0.2	Air	3.70	5.37	48	60	45
0.4	Air	3.67	5.05	100	80	45
0.6	Air	3.67	4.48	157	120	60
0.0	Oxygen	3.8	6.15	− 9	—	—
0.25	Oxygen	3.77	5.7	63	60	40
0.4	Oxygen	3.76	5.1	150	60	45
0.6	Oxygen	3.76	4.83	190	140	60
0.8	Oxygen	6.73	4.91	170	160	55

[a] T_c corresponds to the maximum in $|d\chi_m/dT|$.
[b] T_g corresponds to the maximum in the zero-field cooled χ_m versus T curves.

Figure 11 shows the variation of inverse molar magnetic susceptibility with temperature for $Sr_3Fe_{2-x}Co_xO_{7-\delta}$ ($0 \le x \le 0.8$). Both the Weiss constant θ and the effective magnetic moment μ_{eff} per (Fe, Co) atom obtained from an extrapolation of the data in the high-temperature linear region (220–320 K) are given in Table 1. The θ values for $Sr_3Fe_2O_{7-\delta}$ with $\delta = 0.2$ and 0.26 are, respectively, − 18 and − 9 K, which are in good agreement with previous reports (7); the negative value of θ indicates antiferromagnetic

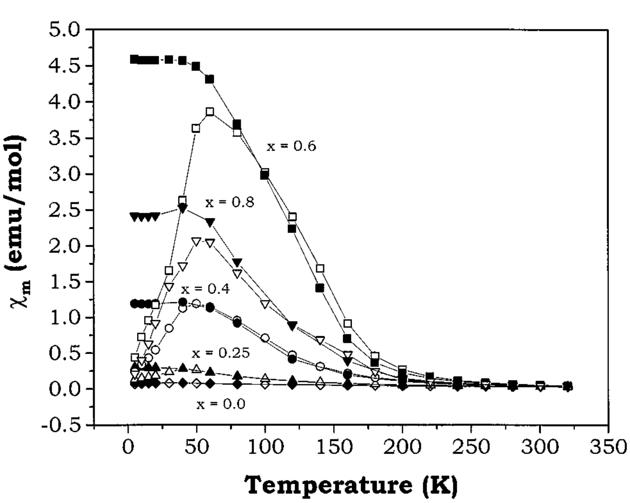

FIG. 10. Variation of molar magnetic susceptibility of oxygen-annealed $Sr_3Fe_{2-x}Co_xO_{7-\delta}$ with temperature. The experiments were carried out with an applied field of 1000 Oe. Solid and open symbols refer, respectively, to field-cooled and zero-field-cooled data.

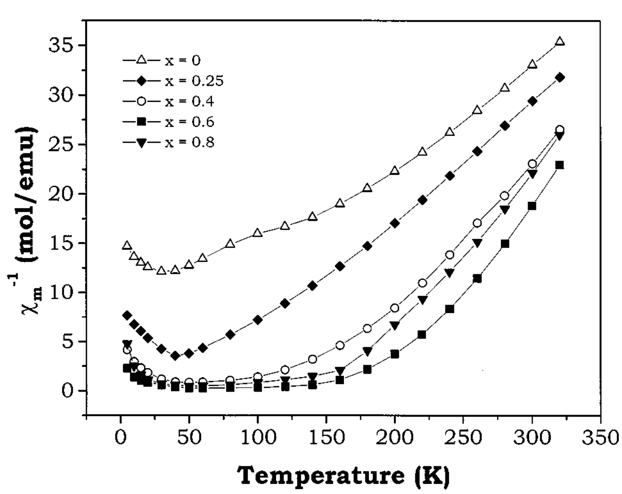

FIG. 11. Variation of inverse molar magnetic susceptibility of oxygen-annealed $Sr_3Fe_{2-x}Co_xO_{7-\delta}$ with temperature.

interactions in the undoped samples with $x = 0$. As the Co content x increases, the slope of the linear region increases and the value of θ becomes positive, suggesting a transition from antiferromagnetic to ferromagnetic correlations. The Weiss constant ($\theta \sim 48$ K) obtained for an air-annealed sample with Co content $x = 0.2$ is remarkably smaller than that reported ($\theta \sim 190$ K) for the same composition with low oxygen vacancy concentration (15). The oxygen vacancies appear to decrease the oxidation state of the transition metal ions and suppress the ferrromagnetic correlation. In the case of the samples with $x \geq 0.4$, the θ values are higher than T_c as expected for ferromagnetic materials.

The μ_{eff} value decreases with increasing Co content for both the air-annealed and oxygen-annealed samples (Table 1). Similar to the Weiss constant θ, the value of μ_{eff} also decreases as the oxygen vacancy concentration δ increases. For a given Co content x, the oxygen-annealed samples have higher μ_{eff} than the air-annealed samples. Assuming that the Fe^{3+} ($t_{2g}^3 e_g^2$) ($S = 5/2$) and Fe^{4+} ($t_{2g}^3 e_g^1$) (S = 2) ions are in the high spin states (24), the decrease in μ_{eff} with increasing Co content may suggest the presence of low spin Co^{III} ($t_{2g}^6 e_g^0$) ($S = 0$) and Co^{IV} ($t_{2g}^5 e_g^0$) ($S = 1/2$) ions rather than high spin Co^{3+} ($t_{2g}^4 e_g^2$) ($S = 2$) and Co^{4+} ($t_{2g}^3 e_g^2$) ($S = \frac{5}{2}$) since the low spin configurations have lower magnetic moment than the high spin configurations. However, the onset of weak ferromagnetism with increasing Co content suggests the nucleation of small regions where ferromagnetic coupling through superexchange interactions involving Co ions in the high spin configurations may be taking place (15, 23, 25, 26). Therefore, both high spin and low spin (or intermediate spin) Co ions may be present in $Sr_3Fe_{2-x}Co_xO_{7-\delta}$.

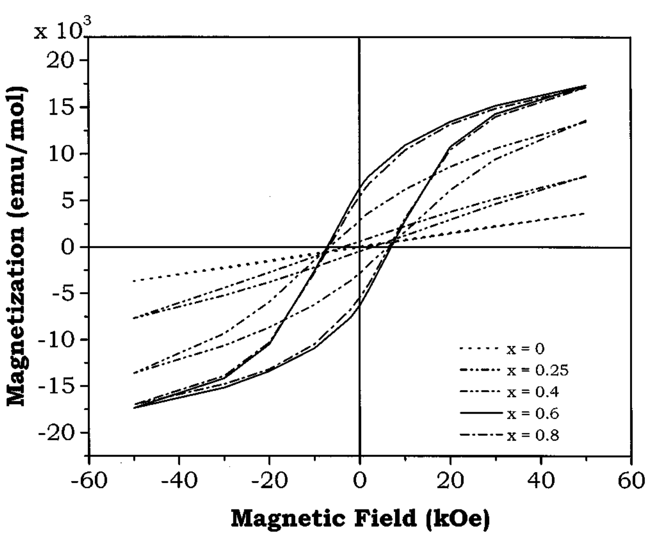

FIG. 12. Variation of zero-field-cooled magnetization with applied field at 5 K for oxygen-annealed $Sr_3Fe_{2-x}Co_xO_{7-\delta}$.

In order to gain more understanding of the magnetic properties, field dependence of the magnetization was studied at 5 K for the zero-field cooled samples. Figure 12 shows the field dependence for the oxygen-annealed $Sr_3Fe_{2-x}Co_xO_{7-\delta}$ samples with $0 \leq x \leq 0.8$. While the $x = 0$ sample shows no hysterisis loop, the samples with $x \geq 0.25$ tend to exhibit loops. As the Co content increases, the loops become more prominent and the coercive field H_c increases and becomes constant around 0.7 T at higher Co contents. However, the spontaneous magnetization is low for all the samples and the magnetization is not saturated even at a field of 5 T (50,000 Oe). This suggests weak ferromagnetism with spin-glass behavior.

4. CONCLUSIONS

$Sr_3Fe_{2-x}Co_xO_{7-\delta}$ samples have been synthesized for $0 \leq x \leq 0.8$. These samples have a tetragonal structure (space group $I4/mmm$) isotypic with the parent $Sr_3Fe_2O_{7-\delta}$. The samples show chemical instability on exposure to ambient air due to reactions with moisture or CO_2. The substitution of Co for Fe decreases the lattice parameters and improves the (Fe, Co)–O–(Fe, Co) covalent interaction resulting in an increase in electrical conductivity. The samples exhibit semiconducting behavior following the relation $\rho \propto \exp(T_0/T)^{1/n}$, but the value of the parameter n increases from 2 to 4 with increasing Co content, suggesting a transition from activated carriers involving a coulomb gap to thermally activated hopping. The samples become weakly ferromagnetic with increasing Co content, suggesting the presence of both low-spin and high-spin Co ions.

ACKNOWLEDGMENTS

Acknowledgment is made to the Welch Foundation (Grant F-1254) for support of this research. One of the authors (F.P.) thanks CONICET, Argentina, for a postdoctoral fellowship.

REFERENCES

1. J. G. Bednorz and K. A. Muller, *Z. Phys. B* **64,** 189 (1986).
2. R. von Helmolt, J. Wecker, B. Holzapfel, L. Schultz, and K. Samwer, *Phys. Rev. Lett.* **71,** 2331 (1993).
3. Y. Teraoka, H. Zhang, S. Furukawa, and N. Yamazoe, *Chem. Lett.* 1743 (1985).
4. S. E. Dann, M. T. Weller, and D. B. Curie, *J. Solid State Chem.* **97,** 179 (1992).
5. P. Adler, *J. Solid State Chem.* **130,** 129 (1997).
6. P. Adler, U. Schwarz, K. Syassen, G. Kh. Rozenberg, G. Y. Machavariani, A. P. Milner, M. P. Pasternak, and M. Hanfland, *Phys. Rev. B* **60,** 4609 (1999).
7. S. E. Dann, M. T. Weller, D. B. Curie, M. F. Thomas, and A. D. Al-Rawwas, *J. Mater. Chem.* **3,** 1231 (1993).
8. J. B. MacChesney, H. J. Williams, R. C. Serwood, and J. F. Porter, *Mater. Res. Bull.* **1,** 113 (1966).
9. D. Samaras, A. Collomb, and J. C. Joubert, *J. Solid State Chem.* **7,** 337 (1973).

10. D. Samaras and R. Chevalier, *J. Magn. Magn. Mater.* **5,** 35 (1977).
11. P. D. Battle, S. K. Bollen, and A. V. Powell, *J. Solid State Chem.* **99,** 267 (1992).
12. F. Prado, T. Armstrong, A. Manthiram, and A. Caneiro. "Ceramic Transactions: Electrochemical Materials, Processes and Devices" (S. K. Sundaram, A. Manthiram, P. N. Kunta, and G. Ceder, Eds.). Am. Ceramic Soc. Westerville, OH, 2001, in press.
13. F. Prado, T. Armstrong, A. Caneiro, and A. Manthiram, *J. Electrochem. Soc.*, in press.
14. T. Armstrong, F. Prado, and A. Manthiram, *Solid State Ionics*, in press.
15. S. Ghosh and P. Adler, *Solid State Commun.* **116,** 585 (2000).
16. R. A. Young, A. Sakthivel, T. S. Moss, and C. O. Paiva Santos, *J. Appl. Crystallogr.* **28,** 366 (1995).
17. A. Manthiram, S. Swinnea, Z. T. Sui, H. Steinfink, and J. B. Goodenough, *J. Am. Chem. Soc.* **109,** 6667 (1987).
18. H. Kobayashi, M. Kira, H. Onodera, T. Suzuki, and T. Kamimura, *Physica B* **237–238,** 105 (1997).
19. L.-W. Tai, M. M. Nasrallah, H. U. Anderson, D. M. Sparlin, and S. R. Sehlin, *Solid State Ionics* **76,** 273 (1995).
20. N. F. Mott, "Metal-Insulator Transitions," 2^{nd} ed. Taylor & Francis, London, 1990.
21. A. L. Efros and B. I. Shklovskii, *J. Phys. C: Solid State Phys.* **8,** L49 (1975).
22. R. K. Li, R. Kremer, and J. Maier, *J. Solid State Chem.* **146,** 488 (1999).
23. R. Mahendiran and A. K. Raychaudhuri, *Phys. Rev. B* **54,** 16044 (1996).
24. A. E. Bocquet, A. Fujimori, T. Mizokawa, T. Saitoh, H. Namatame, S. Suga, N. Kimizuka, Y. Takeda, and M. Takano, *Phys. Rev. B* **45,** 1561 (1992).
25. R. Caciuffo, D. Rinaldi, G. Barucca, J. Mira, J. Rivas, M. A. Señarís-Rodríguez, P. G. Radaelli, D. Fiorani, and J. B. Goodenough, *Phys. Rev. B* **59,** 1068 (1999).
26. M. A. Señarís-Rodríguez and J. B. Goodenough, *J. Solid State Chem.* **118,** 323 (1995).